Photovoltaic effect in CdS-Cu_2S heterojunctions*

K. W. Böer
Institute of Energy Conversion, University of Delaware, Newark, Delaware 19711
(Received 13 October 1975)

The current-voltage characteristic of CdS-Cu_2S solar cells is analyzed in terms of the contributing physical effects. In Cu_2S it is minority-carrier generation and diffusion, in CdS it is a Schottky barrier layer with sliding boundary conditions, $n_j(j)$, and the development of high-field domains which control the current. These domains are responsible for current saturation, but they may also limit the current to a value below the one which can be supplied from Cu_2S, hence they present a ceiling for the observed short-circuit current. The given model is in satisfactory agreement with several experimental observations not previously understood.

I. INTRODUCTION

CdS-Cu_2S solar cells have recently gained renewed interest as a possible device for large-scale terrestrial conversion of solar energy into electric energy.[1] Cells of up to 8.3% conversion efficiency have been made.[2] Open-circuit voltages of 530 mV, short-circuit current densities of 24 mA/cm^2, and fill factors of 75% that different cells have been achieved at air-mass-1 (AM1) (100 mW/cm^2) solar irradiation and cells of (6 ± 0.5)% efficiency can now be produced[2] with a yield in excess of 80%. When properly protected from oxygen and water vapor and kept at temperatures below 60°C these cells have not degraded during more than 2 yr of rooftop deployment and indicate a life expectancy in excess of 20 yr as obtained from accelerated tests at elevated temperatures.[3] There are also industrial estimates published,[4] which indicate that such cells can be produced for less than \$100/kW.

However, the physics of such heterojunctions is yet ill understood. The current-voltage characteristics are described by a semiempirical diode equation, shifted by the short-circuit current j_L,

$$j = j_0(e^{eV/AkT} - 1) - j_L, \tag{1}$$

with

$$j_0 = j_{00} e^{-e\phi/kT} \tag{1'}$$

and A is a factor being 1 or 2 dependent on the type of back diffusion of carriers over the junction and consequent recombination.[5] [Occasionally, A deviates from 1 or 2. Such deviation is commonly explained by series resistance effects, since the open circuit voltage relation obtained from Eq. (1) usually yields $A=1$ or $A=2$ at higher or lower optical excitation rates, respectively.] A band model proposed by Shiozawa[6] is currently accepted which connects a slightly degenerated flat-band chalcocite region (band gap 1.2 eV) through a potential jump ($\Delta E_c \simeq -0.35$ eV and $\Delta E_v \simeq -1.6$ eV) to a space-charge region (diffusion potential $\simeq$0.2 eV) of the CdS (band gap 2.45 eV). It is assumed that essentially all photocarriers are generated minority carriers (n) in Cu_2S.

This model is able to explain a variety of experimental results, however, it poses a number of problems mostly related to understanding the characteristics: Since only a very small fraction of the applied voltage drops across the Cu_2S layer, the observed $j(V)$ must be explained in the CdS region as it interacts with the Cu_2S layer. The parameters of the proper equation governing $j(V)$ should be explained in terms of parameters traceable to a physical model. In order to achieve this we will briefly discuss the physics of the processes involved in the different regions of the cell: Cu_2S, junction region, and CdS.

II. CURRENT TRANSPORT IN Cu_2S PART OF CELL

The copper sulfide layer Cu_xS of more efficient cells has a composition $x > 1.995$ yielding single-phase chalcocite.[7,8] The layer is usually 0.3 μm thick. The average optical-absorption constant[8] for $0.5 < \lambda < 1$ μm is 3×10^4 cm^{-1}. Minority carriers generated in this layer may recombine or diffuse either to the junction or to the outer surface where they contribute to the photocurrent or are subject to surface recombination, respectively. For a layer with minority carrier diffusion length small compared to layer thickness, the carrier profile is shown schematically in Fig. 1. The hatched area indicates the carriers responsible for the photocurrent ($x=0$ is the position of the junction interface, x is negative in Cu_2S and positive in CdS. We have neglected here interface recombination.):

$$j_n = \frac{e}{\tau_n} \int_0^{x(n_{max})} [n_{10} - n(x)]\, dx. \tag{2}$$

The carrier transport in Cu_2S is assumed to be exclusively by diffusion, since any field is deter-

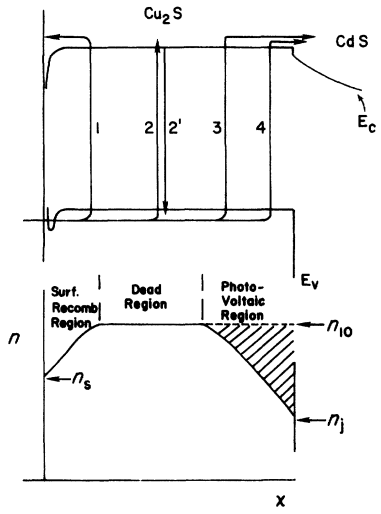

FIG. 1. Schematics of generation, recombination and diffusion in band model (upper part) and electron density profile for $L_n \ll d_1$ (lower part). Hatched area is proportional to photocurrent j_L.

mined by the majority carrier profile which does not change markedly with optical excitation or applied voltage and is unlikely to have the proper profile to contribute markedly to the minority carrier transport for which $n(x)F(x) = \text{const} > j_n$ (diffusion) would have to be fulfilled. [The minority carrier profile $n(x)$ changes, however, with changing operating conditions.]

Hence, one obtains from

$$\frac{dn}{dt} = 0 = g - \gamma np - \frac{1}{e}\frac{\partial j_n}{\partial x}, \tag{3}$$

with g the average generation rate[9,10] (6×10^{21} cm^{-3} sec^{-1} for AM1), γ the recombination coefficient ($\gamma = q\bar{v}_n$), with the effective capture cross section for electrons $q \simeq 3 \times 10^{-18}$ cm^2, assuming for simplicity recombination with holes $p \simeq 3 \times 10^{19}$ cm^{-3}, the thermal velocity $\bar{v}_n \simeq 10^7$ cm/sec, and $\tau_n = 1/\gamma p$ ($\tau_n \simeq 10^{-9}$ sec), for the field-free case

$$\frac{\partial^2 n}{\partial x^2} = \frac{g - n/\tau_n}{\mu kT}. \tag{4}$$

With the boundary conditions $n(x=0) = n_j$ and $n(x=-d_1) = n_d$ with the diffusion length L_n (measured[11] to vary between 1 and 7×10^{-5} cm in these layers), one obtains as solution of (4)

$$n(x) = n_{10} + \frac{n_d + n_{10}[\cosh(d_1/L_n) - 1] - n_{1j}\cosh(d_1/L_n)}{\sinh(d_1/L_n)} \times \sinh\frac{x}{L_n} + (n_{1j} - n_{10})\cosh\frac{x}{L_n}, \tag{5}$$

with

$$n_d = \frac{n_{10}[\cosh(|d_1|/L_n) - 1] - n_{1j}}{es/\beta + \cosh(|d_1|/L_n)},$$

$$\beta = \mu_n kT/L_n \sinh|d_1|/L_n, \quad n_{10} = g_1\tau_n.$$

$n(x)$ is shown for $s = 0$ and for $s = 10^5$ cm/sec in Fig. 2, using $\tau_n = eL_n^2/\mu_n kT$. The current density can be obtained from the derivative of Eq. (5) at $x = 0$, yielding

$$j_n = (e/\tau_n)L_n(n_{1j} - n_{10})\tanh(x_m/L_n), \tag{6}$$

with x_m the position of the maximum of $n(x)$ given by

$$\tanh\left(\frac{x_m}{L_n}\right) = \left[n_{10}\left(\cosh\frac{|d_1|}{L_n} - 1\right)\left(1 + \frac{1}{\alpha}\right) - n_{1j}\left(\cosh\frac{|d_1|}{L_n} - \frac{1}{\alpha}\right)\right] \Big/ \left((n_{1j} - n_{10})\sinh\frac{|d_1|}{L_n}\right),$$

$$\alpha = \cosh(|d_1|/L_n) - es/\beta.$$

This curve j_n is shown in a semilogarithmic plot (j_n vs $\ln n_{1j}$) in Fig. 3 for $s = 0$ and has similarity to the well-known j-V characteristics. (Interface recombination at the junction is neglected. It will be introduced below.)

The current is zero for $n_{j1} = n_{10}$, it is positive for $n_{j1} > n_{10}$ and negative for $n_{j1} < n_{10}$. The negative current increases with decreasing n_{j1} until $n_{j1} \ll n_{10}$, where it saturates. It should be noted, however, that n_{j1} can decrease only to a minimum value $^{\min}n_{j1}$ given by the Richardson-Dushman equation

$$j_n(R - D) = \tfrac{1}{4}e\bar{v}_n(1 - r)\,{}^{\min}n_{j1} \tag{7}$$

(dashed curve in Fig. 3). In the given example $n_{10} \simeq 6 \times 10^{12}$ cm^{-3}, $^{\min}n_{j1} \simeq 4 \times 10^{10}$ cm^{-3}, with negligible reflection at the junction interface ($r \ll 1$).

The saturation current $j_L = j_n(n_{1j} \ll n_{10})$ is plotted

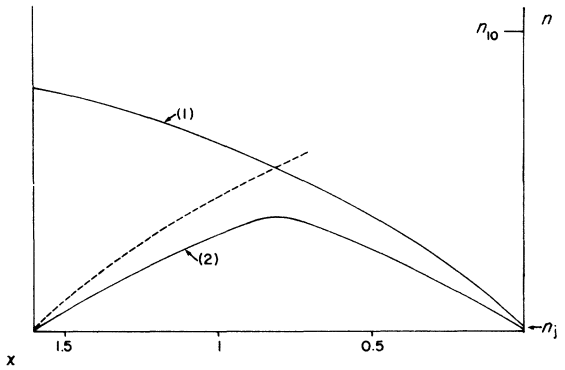

FIG. 2. Electron density profile as calculated from Eq. (5) for $L_n \simeq 1.8 \times 10^{-5}$, $d_1 \simeq 3 \times 10^{-5}$ cm, $\mu_n kT = 1.25 \times 10^{-19}$ A cm^2, $g_1 = 6 \times 10^{21}$ cm^{-3} sec^{-1}, $n_{j1} \simeq 10^{11}$ cm^{-3}. (a) for zero surface recombination, (b) for $s = 10^5$ cm/sec. x measured in units of L_n.

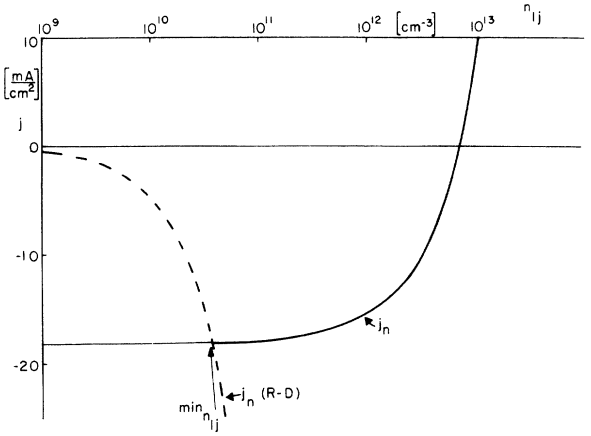

FIG. 3. Diffusion current through Cu_2S as a function of the boundary carrier density (n_{j1}) for zero surface recombination ($x_m = d_1$). Dashed curve is Richardson-Dushman current. Intersect defines $^{\min}n_{j1}$.

in Fig. 4 as a function of L_n:

$$j_L = eL_n g_1 \tanh(x_m/L_n). \tag{6a}$$

The diffusion length depends on the minority carrier life time $L_n = (\mu_n kT\tau_n/e)^{1/2}$, which in turn is related to the majority carrier density p. If one assumes recombination proportional to p (for instance, through shallow recombination centers), with $\tau_n = 1/\gamma p$, one obtains a square-root dependence of j_L on the resistivity ρ

$$j_L = eg(\mu_n\mu_p kT/\gamma)^{1/2}(\rho)^{1/2}\tanh x_m/ (\mu_n\mu_p T\rho/\gamma)^{1/2}. \tag{8}$$

A dependence of j_L on the square root of the sheet

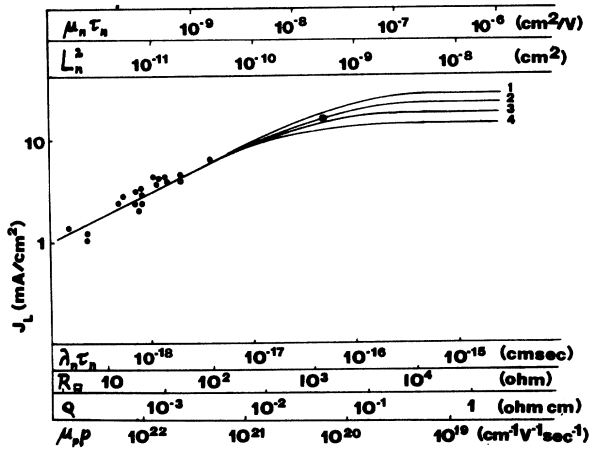

FIG. 4. Saturation current as function of Cu_2S resistivity (ρ) or majority carrier density (p) with measured (Ref. 5) points of sheet resistance [converted to ρ by assuming $d_1 = 3\times10^{-5}$ cm], curves 1–4 are for $x_m = 3\times10^{-5}$, 2.5×10^{-5}, 2×10^{-5}, and 1.5×10^{-5} cm, respectively. For x_m see text, Eq. (12).

resistance $R_\square$ is indeed observed and the curves in Fig. 4 are fitted for best match to the experimental data full circles (the open circle is a datum point from recent high-efficient cells). With an assumed Cu_xS layer thickness of 3×10^{-5} cm one obtains ρ, hence the $\mu_p p$ product.

From these data one concludes that one needs a diffusion length of at least 3×10^{-5} cm to obtain cells with reasonable current output. Assuming that the holes are provided by very shallow acceptors (totally ionized), stemming from copper vacancies, this demands $x > 1.995$, which is also required for single-phase chalcocite. A further increase of x however has to be avoided for reasons of series resistance limitation. From comparison with these experimental data (Fig. 4) one also obtains $p \simeq 5\times10^{19}$ cm^{-3} and $\tau_n \simeq 10^{-9}$ sec, using an estimated $\mu_p \simeq 3$ cm^2/V sec and $\mu_n = 30$ cm^2/V sec, and a capture cross section for electron recombination of $q = 3\times10^{-18}$ cm^2, for 20-mA/cm^2 cells.

III. CURRENT TRANSPORT IN CdS PART OF CELL

In the CdS bulk the electron density n_{20} is considerably larger than n_{10}. Hence one expects a depletion layer in the junction region. In order to determine the properties in this region one must provide the boundary condition for the carriers at the junction interface. It is determined from current continuity and yields the electron density n_{j2} and the field F_{j2} at the junction interface. [For over-all computation instead of F_{j2} a better boundary condition is $\int_0^{d_2}(x)\,dx = V_{\text{appl}} + V_{\text{oc}} - V_D$, with V_{oc} the open-circuit voltage and V_D the diffusion potential given by Eq. (12a).]

In order to proceed, let us first exclude a slab of sufficient width at the boundary between CdS and Cu_2S and assume that the electron density n_{2j} at the CdS side of this slab is given as a linear function of the carrier density n_{1j} at the Cu_2S side of this slab:

$$n_{2j} = \zeta n_{1j}. \tag{9}$$

We will justify this assumption later. It will also be seen that ζ is of the order of 1.

The field at the interface may be obtained by integrating Poisson's equation (index 2 refers to the CdS region):

$$\frac{\partial F}{\partial x} = \frac{e}{\epsilon\epsilon_0}[n(x) - n_{20}]; \tag{10}$$

for $n(x) \ll n_{20}$, and neglecting recharging of traps,

$$F_{j2} \simeq [(2n_{20}e/\epsilon\epsilon_0)V_D]^{1/2}. \tag{10a}$$

From the transport equation with $j = 0$ one obtains for the diffusion potential

$$V_D = (kT/e)\ln(n_{20}/n_{10}\zeta). \tag{10b}$$

The expected electron density, potential, and field profiles are drawn schematically in Fig. 5 for $\zeta = 1$. The solutions of Poisson and transport equations are discussed in one relevant direction with $\vec{F} = (-F_x, 0, 0)$ and $\vec{j} = (-j_x, 0, 0)$. In the Cu_2S region the electron transport is exclusively determined by diffusion. In CdS the drift is equal or nearly equal to the diffusion at or in the neighborhood of the open-circuit voltage point. For positive currents the diffusion exceeds the drift; for negative currents the drift exceeds the diffusion (in the CdS bulk, however, always electron drift prevails). As long as $j_n \ll (j_{\text{drift}}, j_{\text{diffusion}})$, one can easily integrate the transport equation:

$$j_n = e\mu nF + \mu kT\frac{dn}{dx}, \tag{11}$$

yielding

$$n_{2j} = n_{20}e^{eV_D/kT}, \tag{11a}$$

and obtains with Eqs. (6) and (9) and normalization of $V = V_{\text{appl}}$ (measured from V_{oc})

$$j_n = \frac{e}{\tau_n}L_n N_{c2}\tanh\frac{x_m}{L_n}\exp\left(-\frac{e(\tilde{V}_D + V_{oc})}{kT}\right)$$

$$\times\exp\left(\frac{eV}{kT}\right) - \frac{eL_n n_{10}}{\tau_n}\tanh\frac{x_m}{L_n}, \tag{12}$$

with

$$\tilde{V}_D = \frac{kT}{e}\ln\frac{N_{c2}}{n_{20}} + V_D = \frac{kT}{e}\ln\frac{N_{c2}}{n_{1j}\zeta} \tag{12a}$$

(attention should be given to a mixed set of parameters: N_{c2} and $\tilde{V}_D$ in CdS, and τ_n, L_n, n_{10}, x_m in Cu_2S).

This equation describes within the experimental error the observed behavior [Eq. (1)] at applied voltages near V_{oc}, with

$$j_{00} = (e/\tau_n)L_n N_{c2}\tanh(x_m/L_n) \simeq 10^4\ \text{A/cm}^2,$$

$$\Phi = \tilde{V}_D + V_{oc} \simeq 0.85\ \text{eV},$$

$$j_L = eL_n g_1\tanh(x_m/L_n) \simeq 20\ \text{mA/cm}^2.$$

It should be noted that in contrast to the above values the classical junction theory yields $j_0 = e\bar{v}_n N_c \simeq 5\times 10^6\ \text{A/cm}^2$ and $e\phi \simeq E_{g1} \simeq 1.2\ \text{eV}$, values which are considerably higher than experimentally observed.

At applied voltage sufficiently below V_{oc}, when current saturation starts to become observable, the drift current in CdS must exceed the diffusion current to the degree that the latter can be neglected. Here the integration of (11) for $j_n = 0$ is no longer permitted. The barrier layer is pulled open and F_{j2} usually has reached values above 30 kV/cm and cannot increase much further without first causing field excitation and then tunneling to occur (this would cause the current to increase rather than to saturate). The observed current saturation shows that the field F_{j2} must be limited, say to a value F_c, assumed to be 50 kV/cm. (The selection of a specific F_c is not critical for the following argument: As long as this field increases with monotonically increasing slope towards the junction interface, at best 0.4 V can drop across the barrier layer.)

A rapid current increase in reverse direction is indeed observed in all CdS-Cu_2S solar cells before they are exposed to certain heat treatments (see, e.g., curve 1 in Fig. 10). The desired extensive current saturation appears only after a heat treatment at sufficient temperature and length (typically at least 2 min at 250 °C, 30 min at 180 °C or 18 h at 130 °C—see Fig. 10). During such a heat treatment copper diffuses[12,13] into a layer of about 2×10^{-5} cm thickness. It was proposed[6] to make this copper diffusion responsible for a so-called i layer across which the voltage could drop by at least 1 V as observed in reverse direction during current saturation.

It is however evident (see Sec. IIIA) that Poisson and transport equation for electron currents do not include solutions which permit such a large voltage drop and keeping a monotonic behavior of $n(x)$ without resorting to high-field effects.

The high-field effect which is observed[14] to occur at lowest fields is field quenching[15] in photoconducting CdS. It requires optical excitation, creating holes *and* electrons in CdS, and sensitization, since (field) quenching describes a transition from a high (sensitized) to a low (nonsensitized) carrier life time state (the transition caused by the electric field). Sufficient optical excitation (with a generation rate $g_2 \simeq 10^{18}$–$10^{20}\ \text{cm}^{-3}\text{sec}^{-1}$) is present near the junction and sensitization is achieved by the copper diffusion described above. Hence effects related to field quenching—such as the formation of *high-field domains*[6] are expected in this region if the field becomes high enough and other effects, such as electron injection from the Cu_2S layer do not prevent their formation.

It can be easily seen that less than 0.2 V below V_{oc} the maximum field at the junction interface must exceed 10^4 V/cm (using a simple Schottky-barrier estimation and a space charge of $\sim 10^{16}$ to $10^{17}\ \text{cm}^{-3}$, as obtained from capacitance measurements[10] near V_{oc}), hence sufficient fields to initiate field quenching are expected.

Electron injection from Cu_2S could only modify the picture if it causes a marked increase in majority carrier density.[16] This is not the case—however needs further analysis provided in Sec.

III B.

Without limiting the field near the junction interface by such high-field domains below the tunneling field to extract electrons from the valence band of Cu_2S into the conduction band of CdS, the reverse breakdown is estimated to start only a few tenths of 1 V below the open circuit voltages. This would substantially reduce the fill factor of the characteristics and rapidly force the current to enter the third quadrant (as soon as $j > j_L$).

It is therefore suggested to consider field quenching inducing a negative differential conductivity range in CdS and in turn causing high-field domains as being essential to explain the photovoltaic effect with extended current saturation in CdS-Cu_2S heterojunctions.

Let us now continue the more detailed analysis of the barrier layer with reverse bias after $n(x=0)$ has already dropped substantially (curve 3) from the open circuit condition (curve 2—see Fig. 5).

A further increase in voltage drop across the junction can then only be accommodated by widening the junction—hence lowering the gradient of n near the junction interface. The dashed curves in Fig. 5 presents a typical case as expected in the saturation range. Here the field and carrier density remains nearly constant (at $F_{j2} \simeq F_c$ and $n \simeq n_{j2}$) and the current is given by

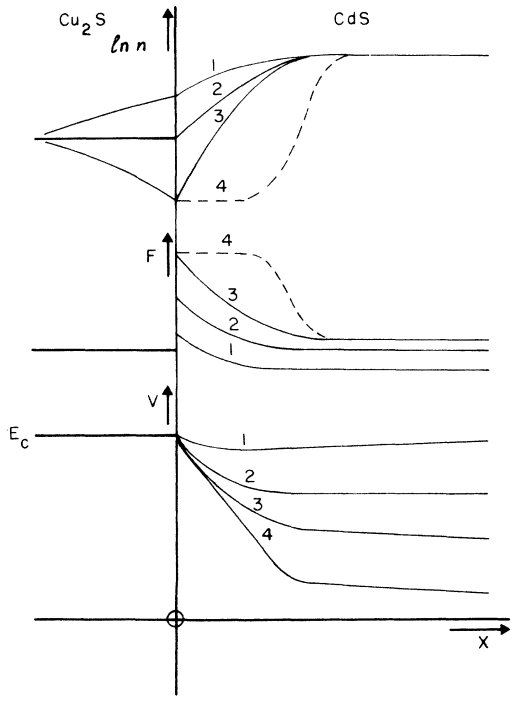

FIG. 5. Electron density, field, and potential distribution in a CdS-Cu_2S heterojunction at different currents; curves (1) forward, (2) open circuit, (3) slight reverse (near maximum power point), (4) saturation range.

$$j_n = e\mu_n n_{j2} F_{j2}; \tag{13}$$

j_n is independent of the applied voltage if F_c is (i.e., the current saturates). For high-field domains this is indeed fulfilled.

The voltage drop across such a high-field domain of width x_2, which widens as the voltage increases, is given by

$$V = F_{j2}x_2 + F_{20}(d_2 - x_2) \simeq F_{j2}x_2, \tag{13a}$$

with $F_{20} = j_n/\sigma_{n2} \lesssim 1$ V/cm for $\sigma_{n2} \gtrsim 10^{-2}\Omega^{-1}\,\mathrm{cm}^{-1}$. The width x_2 of the domain is estimated to be in the 10^{-5}-cm range for $F_c \simeq 50$ kV/cm (x_2 cannot easily be obtained from capacity measurements since for domains the total space charge remains constant; the regions of positive and negative space charge are only pulled further apart, leaving their magnitude nearly unchanged. The observed[9] slowly changing capacity in the current saturation range may be direct evidence for such domains).

A. Field of direction analysis

Whenever carrier density and field are nearly constant, then $\partial n/\partial x \simeq \partial F/\partial x \simeq 0$ and the solution of transport and Poisson equation is near a singular point.[14] In Eqs. (9) and (11) only one singular point at n_{20}, F_{20} is contained. This can best be seen by rewriting Eqs. (10) and (11) as

$$\frac{dF}{dx} = \frac{e}{\epsilon\epsilon_0}[n(x) - n_{20}], \tag{14a}$$

$$\frac{dn}{dx} = \frac{1}{\mu kT}(j_n - e\mu nF), \tag{14b}$$

and discussing all possible solution curves of Eqs. (14) as their projection into an arbitrary nF plane. [This is permitted since Eqs. (14) do not contain x explicitly and fulfill a Lipschitz condition.[17]] All possible solutions are represented in such an nF plane and can be constructed by following from a certain point given by the boundary condition, say $n(x=0)$ and $F(x=0)$ along the slope through this point to the next point in this plane and along its slope to the next and so forth until the solution curve is completed. Since through every point of the nF plane goes one and only one solution (i.e., slope), such solution curve is uniquely determined (there are no solution curves crossing each other).

Obviously it is quite cumbersome to draw such a field of slopes (Fig. 6) for every specific case and to obtain solutions of a given problem in such a way. (For better conceivability, in Fig. 6 instead of slopes the directions are drawn: the arrow points towards increasing x, i.e., towards the anode.)

Of great assistance is the introduction of two

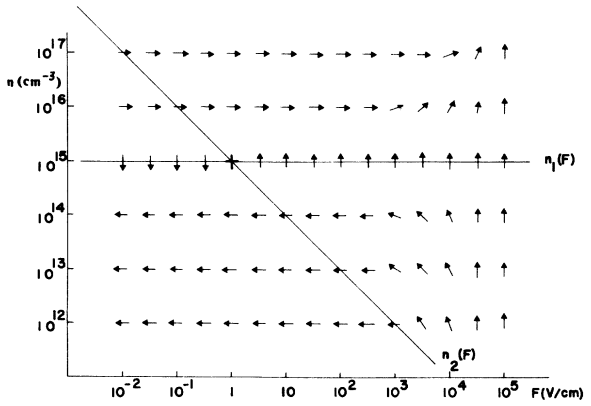

FIG. 6. Field of direction for Eqs. (14) calculated for $j_n = 20$ mA/cm^2, $\mu_n = 60$ cm^2/V sec, $\epsilon = 10$, $T = 300$ °K and $n_{20} = 10^{15}$ cm^{-3}. $n_1(F)$ and $n_2(F)$ are quasineutrality and drift current curves, respectively (see text). The intersection of n_1 and n_2 is the only singular point contained in Eqs. (14) with field-independent parameters.

auxiliary curves:

$$n_1(F), \quad \text{for which } \frac{dF}{dx} \equiv 0,$$

and

$$n_2(F), \quad \text{for which } \frac{dn}{dx} \equiv 0.$$

$n_1(F)$ is also referred to as neutrality curve (since here the space charge vanishes) and $n_2(F)$ as drift current curve [see Eq. (14b)]. These curves are shown in Fig. 6 and divide the field of slopes (field of directions) into four sectors, dependent on the sign of these derivatives. Each sector represents one quadrant of direction; e.g., above $n_1(F)$ and $n_2(F)$ the slopes dn/dx and dF/dx are positive, hence all directions in this sector must be in the first quadrant, i.e., between 0° and 90°. Representing this sector by a short arrow pointing right and up; the other sectors can be presented by short arrows as shown in Fig. 7.

With the aid of these two curves the discussion

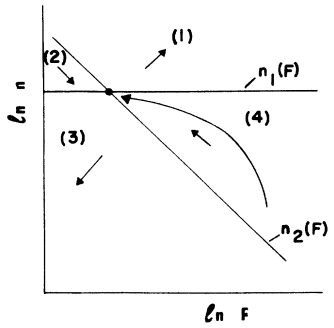

FIG. 7. Simplified field of direction of Eq. (14). The curved arrow represents a possible solution curve.

of possible solutions of the transport and Poisson equation is considerably simplified. One sees immediately that only one singular point exists as intersection of n_1 and n_2, and this singular point is a saddle point, i.e., only solutions from the sectors (2) and (4) (Fig. 7) can approach the singular point.

Such solutions are the only ones of interest for semiconductors long compared to the Debye length. With a charge density of at least 10^{15} cm^{-3}, the Debye length of less than 2000 Å is indeed small compared to the thickness of the CdS ($d_2 \simeq 2 \times 10^{-3}$ cm). A typical solution[18] (long curved arrow in Fig. 7) is shown as curve 3 in Fig. 5. However, as pointed out earlier, the voltage drop across the barrier for any solution of the type given by curve 3 can account at best for 0.4 V:

$$\Delta V_{\max} \simeq (kT/e) \ln n_{20}/{}^{\min}n_{j1}\xi. \qquad (15)$$

The additional voltage drop in CdS and Cu_2S is negligible. There is no other solution contained in Eq. (4) which can provide a substantially higher voltage drop as can best be seen from Fig. 6: If one relaxes the condition (9) and permits n_{j2} to drop further, the boundary value is certainly limited by $n_2(F)$ and $F = F_{\max}$ at which breakdown occurs. With $F_{\max} < 10^6$ V/cm one obtains ${}^{\min}n_{j2} > 10^9$ cm^{-3}, and with $n_{20} \simeq 10^{17}$ cm^{-3} one concludes that an upper limit of 0.5 V presents the maximum voltage drop possible. The current voltage curve, however, requires a saturation range of at least 1.5 V. [Current saturation itself is not contained in Eqs. (14) with field-independent parameters.]

There is no way in which this voltage drop and current saturation can be accommodated within the given model with field independent parameters (one may note that a similar statement holds for the simple Schottky barrier in a homogeneous semiconductor, and pronounced diode behavior indicates a similar need for expansion of the diode theory). *One therefore must assume an additional mechanism, which permits the flattening of n(x) and F(x) near the junction boundary. Such a mechanism must reduce the μn product with increasing field stronger than linearly.*[17,19] Only this could provide a second singular point and could accommodate several volts as required by the experimentally observed jV characteristic in the saturation range.

Field-quenching[15] in photoconductive CdS is one possible mechanism. It is observed[15,20] to occur at fields of approximately 50 kV/cm in Ag- or Cu-doped CdS and causes the density of photogenerated carriers to drop by at least three orders of magnitude when the field reaches 30–60 kV/cm.

With such effect n in Eq. (14a) can be replaced by $n_1(F)$ which may be approximated by (see Fig.

8)

$$n_1(F) = g_2\left\{\gamma_s p_s + \frac{\gamma_f p_f}{2}\left[1+\tanh\left(\frac{F-F_c}{\alpha F_c}\right)\right]\right\}^{-1} \qquad (16)$$

(index s and f representing slow and fast centers, respectively), with α a parameter to provide a reasonable match to the experimentally observed quenching transition. [A better match can be obtained when the unmasking of the fast transition via redistribution of holes is properly taken into consideration. However, the expression is lengthy. Equation(16) is sufficient for most purposes.]

The field of direction now provides the possibility for two singular points (Fig. 8—a third singular point in Fig. 8 is of no consequence to our solution). A solution extending between the vicinity of these two singular points (curved arrow in Fig. 8) has the desired behavior as shown by the dashed curves 4 in Fig. 5. The current is given essentially by electron drift [Eq. (13)] in the junction region (near singular point II), than by drift and diffusion (transition region), and again by drift in the CdS bulk (near singular point I). [Figure 8 applies only to the Cu-doped (sensitized) part of the CdS. Another transition of minor importance occurs towards the semiconducting bulk of the CdS with $n_{20s} \simeq 10^{15}$–10^{17} cm^{-3}.]

As long as the high-field region (usually referred to as a high-field domain[14,17,19]) can expand, the current remains the same. Current saturation is

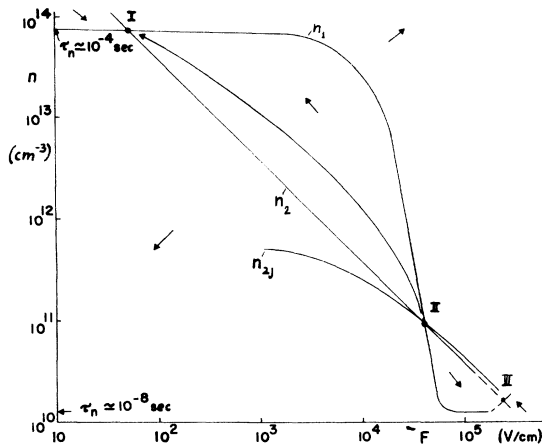

FIG. 8. Simplified field of direction for modified Eq. (14) with field-dependent recombination parameters (implicit in Poisson equation). Three singular points (I, II, III) are possible. Curved arrow represents a domain-type solution. $n_1(F)$ is given by Eq. (16) for field quenching (transition from slow to fast recombination traffic). The values used in Eq. (16) are $\gamma_s p_s = 10^4$ sec^{-1}, $\gamma_f p_f = 4\times 10^7$ sec^{-1}, $g_2 = 10^{18}$ cm^{-3} sec^{-1}, $\alpha = 0.2$, $F_c = 50$ kV/cm, and for $n_2(F)$ the values used are $j_n = 20$ mA/cm^2 and $\mu_n = 30$ cm^2/V sec. For n_{2j} see text and Eq. (13b).

observed. This effect of field quenching limits the field to a critical value, $F_c = F_{II}$, and is well-known cause for high-field domains and current saturation[19] in photoconducting CdS.

It should be noted that current saturation comes into this picture as a by-product of the high-field domain. Field and carrier density[21] at the boundary becomes locked close to the values at the singular point, and Eq. (13) determines consequently the saturation current.

This seems to be in contradiction with the current analysis in the Cu_2S part of the cell, where Eq. (8) determined the saturation current. Hence one needs a better analysis how the CdS and the Cu_2S parts are connected to each other.

B. Photocarrier injection into high-field domain

The electrons which are generated in the adjacent Cu_2S are injected at the junction boundary into the CdS. Since essentially none of the holes from the Cu_2S can penetrate the high barrier into the CdS (see Fig. 12), the *injected* electron current remains constant throughout the CdS as long as no holes from the CdS-metal contact can reach the junction region. Since the field in the CdS bulk is small ($\lesssim$1 V/cm) such injection is indeed negligible.

The flux of injected electrons consequently determines the boundary density, n_{1j} at the junction interface, providing the boundary condition for Eqs. (14) (however with field-dependent parameters—see Sec. IV) in CdS.

As shown in Sec. II, Eq. (6), n_{1j} is a function of the current density, yielding $\zeta n_{2j}(j_n)$. Assuming predominant carrier drift in CdS at the junction interface, the locus of this boundary density in the n-F plane is given by

$$n_{2j} = \frac{\zeta n_{10}}{1+\mu_{n2}F_{j2}(\tau_{n1}/L_{n1})\coth(x_m/L_n)} \qquad (13b)$$

and is drawn in Fig. 8 for $\zeta = 0.3$ (see Sec. IV), and $L_{n1}/\mu_{n2}\tau_{n1}\coth(x_m/L_{n1}) = 7600$. The curve $n_{2j}(F)$ intersects $n_1(F)$ at $F_{II} \simeq 40$ kV/cm. $n_1(F)$ is drawn for reasonable electron lifetimes $\tau_n = 10^{-4}$ sec in the sensitized and $\tau_n = 10^{-8}$ sec in the quenched case,[22] assuming an effective generation rate in CdS of $g_2 \simeq 10^{18}$ cm^{-3} sec^{-1}.

One sees that similarly to the well studied negative differential conductivity case in bulk CdS,[14,17,19,20,22] the boundary condition of carrier injection from the Cu_2S provides the necessary provision for $n_{2j}(F)$ to force the development of simple (starting at the junction interface near the singular point II) high-field domains as long as $n_{2j}(F)$ and $n_1(F)$ cross. As shown above that is

indeed the case for reasonable parameter combinations.[21]

IV. CdS-Cu_2S INTERFACE REGION

The understanding of this interface region is crucial for providing the proper boundary conditions for each material. We will deal with this region as a slab of finite thickness W of a third material (the interface material). For reasons to be explained below we will assume that this slab lies within the Cu_2S lattice with only one surface coinciding with the Cu_2S-CdS interface. This slab will contain additional recombination centers of density N_r (cm^{-3}), part of which are presumed to be caused by the lattice mismatch dislocation field of density 1.95×10^{12} cm^{-2} perpendicular to c, yielding a dangling bond density of

$$1.07\times10^{14}\ cm^{-2}.$$

This slab will also contain a net negative space charge of approximately 10^{12} cm^{-2} to accommodate the field jump at the interface (from $<10^{-2}$ V/cm in Cu_2S to $\simeq 50$ kV/cm close to the interface in CdS).

The current through the CdS part of the cell can consequently be described as the net difference between the electron diffusion current in Cu_2S entering this slab and the recombination current

$$j_{n2}=j_{n1}-j_R=e\{n_{j1}[(L_{n1}/\tau_{n1})\tanh(x_m/L_{n1})+s_j] - n_{10}(L_{n1}/\tau_{n1})\tanh(x_m/L_n)\}, \tag{17}$$

with s_j, the interface recombination velocity,

$$s_j=\bar{v}_n S_f \tag{18}$$

and S_f, the "surface fill factor,"

$$S_f=q_s N_R W, \tag{19}$$

with q_s the capture cross section for electrons of recombination centers N_R in the interface slab.

Figure 9 illustrates Eq. (17): curve 1 shows j_{n2} for zero recombination for a diffusion velocity $v_{D1}=L_{n1}/\tau_{n1}\simeq 2\times10^4$ cm/sec and $n_{10}=6\times10^{12}$ cm^{-3}. Curves 2 and 2′ are the recombination currents for $S_j=2\times10^4$ cm/sec and $s_j=4\times10^4$ cm/sec, respectively, and curves 3 and 3′ are the resulting net currents j_{n2} with recombination. It is evident that the saturation current j_L is not markedly influenced but the open circuit voltage is reduced according to

$$\delta V_{oc}=(k\tau/e)\ln(n_{1j0}/n_{1jR}), \tag{20}$$

with

$$n_{1jR}=n_{1j0}v_{D1}/[v_{D1}+s\coth(x_m/L_n)].$$

The consideration of a recombination current results in a reduced boundary electron density. At open circuit condition a finite electron current in Cu_2S towards the junction interface is exactly compensated by a hole current of opposite sign and is equal to the recombination current j_R.

It should, however, be noted that one starts at V_{oc} with a smaller electron density n_{1jR} (instead of $n_{1j}=n_{10}$), hence the range from n_{10} to ${}^{\min}n_{j1}$ [Eq. (7)] is reduced. Consequently j_L will be also reduced as soon as n_{1jR} approaches ${}^{\min}n_{j1}$. This limits the yet unknown interface recombination velocity to

$$s\le V_D[(n_{10}/{}^{\min}n_{j1})(j_L/j_{L_m}-1)-1], \tag{21}$$

with j_{L_m} the maximum current density for a collection efficiency of one (36 mA/cm^2 for AM1 excitation). With $v_D=2\times10^4$ cm/sec, $n_{10}/{}^{\min}n_{j1}=100$ and $j_L/j_{L_m}=0.6$ for good present cells, one concludes $s\le 8\times10^5$ cm/sec. However, this leaves a range n_{1jR} to ${}^{\min}n_{1j}$ of only 2.5, hence a very abrupt transition to current saturation which is not observed. A more reasonable upper limit for s is 10^5 cm/sec for the conditions otherwise given above.

The maxium reduction of the open-circuit voltage caused by interface recombination can be estimated from eqs. (20) and (21) and is 0.1 V. The interface recombination is consequently a minor effect for better cells currently produced.[2]

A. Band interconnection

The connection between the bands of the Cu_2S and CdS is cause of a controversy. Proponents of a spikelike connection of the conduction band cite evidence of tunneling, proponents of a jumplike connection cite low ϕ values with dominant recombination current and inference of indirectly measured difference in electron affinities. Both arguments are inconclusive.

Sufficient knowledge about the different currents will settle this argument. However, already with the present knowledge one recognizes that the electron flux across the junction interface is substantially larger than the hole flux. If we neglect the hole contribution, then energy and momentum conservation dictates continuity of Fermi level and conduction band, e.g., electron current continuity in forward direction for $n_{2j}>n_{10}$ cannot be maintained otherwise. A small hole flux may modify this condition slightly. We will return to it in Sec. IV B.

Another modification is given by the differences in band structure $E(k)$ in both materials. An electron passing through the interface will consequently experience a change in k, hence a partial reflection like a photon passing from one medium into another. Near the band edges it seems sufficient to account for such differences by an effective mass

approximation resulting in [see Eq. (9)]:

$$n_{2j}/n_{1j} = (m_{n2}/m_{n1})^{3/2}. \quad (22)$$

The effective mass of electrons in Cu_2S is unknown. It is probable that it is of the same order as the effective mass of electrons in CdS: $m_n(\text{CdS}) = m_{n2} = 0.2m_0$.

One concludes that the electron density at the CdS side of the CdS-Cu_2S junction interface is probably slightly lower than at the Cu_2S side as calculated with neglection of interface recombination. The factor ζ [see Eq. (9)] which represents this relation is probably smaller than one, and probably also larger than 0.1. For purposes of definiteness it is assumed to be $\zeta = 0.3$.

B. Hole current in junction region

There are two contributions to the hole current: (i) The hole current in Cu_2S which is equal to the recombination current and closes the loop between pair generation, electron diffusion towards the junction, and recombination at the junction interface. This hole current does not cross the interface. Its influence was implicitly discussed in Sec. IV (recombination). (ii) The hole current which stems from holes generated by light in CdS and diffusing and drifting towards the interface. (Since the field is essentially determined by electrons, this field helps hole drifting towards the junction.) This current crosses the junction interface together with an appropriate flux of electrons (equal flux for open circuit condition). It is this current which may influence slightly the boundary condition for connecting valence and conduction bands. However, we will neglect this effect for the purpose of this paper.

For reasons of coupled carrier flux a slight increase in open circuit voltage is expected, the magnitude of which can be estimated[23] from $j_{n2}^* = j_{p2}$, with $j_n^* = \mu_n n^* dE_{F_n}/dx$, with asterisks indicating the partial electron flux. Using a Schottky-barrier approach (near V_{oc} justified) one obtains

$$\Delta V_{oc} \simeq \frac{1}{e}\Delta E_{F_n} = \int_0^{L_{p2}} \frac{j_{p2}}{e\mu_{n2}n_{Lp2}} \exp\left(-\frac{x^2}{L_{D2}^2}\right) dx$$

$$\simeq 0.8\frac{L_{D2}j_{p2}}{e\mu_{n2}n_{Lp2}}, \quad (23)$$

with L_{D2} the Debye length in the CdS side of the junction. Using $L_{D2} \simeq 3\times 10^{-6}$ cm, $\mu_{n2} = 100$ cm^2/Vsec, $n_{Lp2} = n(x = L_{p2}) \simeq 10^{13}$ cm^{-3}, and $L_{p2} \simeq 10^{-5}$ cm, one estimates $\Delta V_{oc} \simeq 10^{-2} j_{p2}$, hence negligible for all practical purposes.

V. CURRENT-VOLTAGE CHARACTERISTICS

The current through the CdS-Cu_2S solar cell is determined by the applied voltage which causes a redistribution of electrons in the barrier layer of the CdS, and by the optical excitation which provides a reservoir of electrons in the Cu_2S. Both regions are coupled by the electron density at the CdS-Cu_2S boundary. This is a gliding boundary condition with $n_{2j} = \zeta n_{1j}(j)$ given by Eqs. (6) and (9) with $\zeta \simeq 0.3$. Because of difficulties to integrate the transport equation, the current-voltage characteristic can not be given as a polynomial of well tabulated functions; but it can be approximated by Eq. (12) in the vicinity of the open-circuit voltage, and by Eq. (13) in the saturation range. This saturation range is responsible for the extended flat saturation of the current-voltage characteristics of well performing CdS-Cu_2S solar cells. The current in this range ($\simeq$ short-circuit current) must therefore lie below the extraction saturation current given by Eq. (8). Hence it seems to be most important to match the relevant properties of CdS and Cu_2S so that the domain saturation current in CdS is as close as possible to the extraction saturation current.

In summary, we propose to explain the j-V characteristic in the following manner:

(i) At V_{oc} and negligible surface and junction interface recombination the electron density in Cu_2S is constant at $n_{10} \simeq 5\times 10^{12}$ cm^{-3} (for AM1), in CdS it increases from $\simeq 0.3n_{10}$ at the boundary to n_{20} in the bulk with drift and diffusion current balancing each other in the junction region.

(ii) At V_{oc} and with finite surface recombination the electron density has a maximum near the center plane of the Cu_2S layer and decreases towards the surface and towards the junction interface proportional to the respective surface recombination velocities. The electron diffusion currents towards these surfaces are exactly compensated by corresponding hole currents. In the CdS the behavior is similar to (i), however with n_{2j} starting at a lower boundary density ζn_{1j} (the corresponding field is consequently larger at $x = 0$).

(iii) At $V \lesssim V_{oc}$ electron diffusion carries the current from the Cu_2S into the CdS with $n_{j1} < n_{10}$. In CdS the current is carried by the difference of diffusion and drift, the latter being slightly larger. The current is negative and is limited by extraction saturation when $n_{j1} \ll n_{10}$.

(iv) With finite recombination at the junction interface part of the diffusion current from Cu_2S is diverted back into the Cu_2S via recombination and does not reach the CdS. With approaching current saturation the recombination current decreases as the electron density at the junction does. Recombination does reduce the open circuit voltage (up to 0.1 V) but has less influence on the short-circuit saturation current.

(v) However, before extraction saturation is

reached n_{j2} may equal a critical density n_{II} in CdS (corresponding to F_{II} and carrier drift). Now current saturation occurs because of high-field domains in CdS. It produces a ceiling for the current which otherwise could increase to the value supported by minority carrier extraction from Cu_2S [Eq. (8)]. The highest saturation current can be obtained when n_{II} equals the Richardson-Dushman limit $^{min}n_{j1}$.

(vi) At applied negative voltages of sufficient magnitude (usually < -2 V) the current starts to increase rapidly. Tunneling from the Cu_2S valence band into the CdS conduction band may be reason for the observed reverse breakdown. (Tunneling probably through weak spots of the cell, since tunneling through a domain cannot occur for reasons of insufficient F_{II}).

(vii) In forward direction ($V > V_{oc}$) the current increases exponentially. In the CdS junction and in Cu_2S it is carried by diffusion (near V_{oc} in CdS by the balance of drift and diffusion with the latter being slightly larger). In the CdS bulk it is carried by drift.

(viii) With recombination the majority of the current from CdS into Cu_2S may be carried by the recombination through the interface and by hole drift in Cu_2S. However current continuity of the electron current requires that part of this current is also carried through the Cu_2S conduction band as soon as the electron density at the interface has risen above n_{10}.

(ix) If the CdS is not properly sensitized (e.g., copper doped) at least in the junction region, high-field domains can not develop and consequently the field at the junction is not limited to values in the 50-kV/cm range but can increase further. If other field-limiting effects are absent until tunneling fields are reached, the characteristic will not show a pronounced saturation range but the (negative) current will rapidly increase with increasing (negative) applied voltage (see Fig. 9).

With high-field domains acting as a ceiling for the current saturation one may ask whether this presents an upper limit necessarily below the saturation carrier extraction for the Cu_2S. With $^{min}n_{1j} \simeq 10^{11}$ cm^{-3} for the highest expected j_L (36 mA/cm^2), one estimates a $\mu_n F_{II}$ product (assuming $\zeta = 0.3$) of approximately 6×10^6 cm/sec. With a mobility of nearly[21] 100 cm^2/V sec one estimates maximum fields of $F_{II} \simeq 60$ kV/cm which are well within the domain range for F_{II}. Hence fine tuning of the pertinent properties should permit us to reach such saturation currents.

VI. SOME EXPERIMENTAL FACTS

In nonsensitized (undoped) CdS field quenching is not expected. (Quenching is defined as transition from the sensitized, highly photoconductive state to a state in which recombination through fast centers dominate. In a nonsensitized cell only the fast recombination determines the carrier lifetime, hence a further reduction is not expected.) It may hence be concluded that in such undoped CdS the field can increase further with applied voltage and reach the tunneling field, at which — without saturation — the current increases rapidly via tunneling of valence electrons from Cu_2S into the conduction band of CdS.

It is indeed observed that the j-V characteristic of a freshly prepared CdS-Cu_2S solar cell shows no current saturation (Fig. 10 — curve 1). Only when the cell is sufficiently heat treated to permit copper diffusion into a slab of at least a few thousand angstrom thickness, is a saturation range observed (curves 2 and 3 of Fig. 10). Estimated domain thickness[16] [Eq. (13a)] and the thickness of the copper-doped region as obtained from diffusion data[12] agree within the experimental error.

The limitation of j_L presented by high-field domains seems to explain the observation that usually the spatial distribution of j_L over an entire CdS-Cu_2S solar cell, as obtained with a scanning light spot, is highly uniform for good cells [Fig. 11(a)], in spite of the fact that L_n is observed[10] to vary considerably (by a factor of 2–3) over the cell. If inhomogeneities are observed, they appear usually as dimples below the ceiling rather than protrusions above the ceiling. One may conclude that the copper doping and field quenching limits the current and is less sensitive to structure inhomogeneities than the diffusion length.

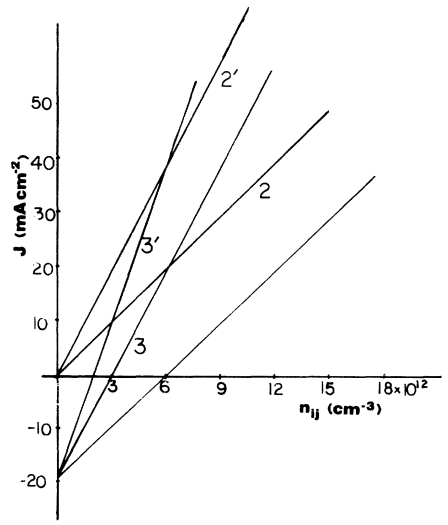

FIG. 9. Different currents at junction interface as function of the electron density at the junction ($\zeta = 1$ assumed for simplicity). For explanation see text.

This picture seems to be supported by a rather profiled scan before heat treatment [Fig. 11(b) — slight heat treatment as applied during grid lamination are often sufficient to transform the profiled scan in a more uniform scan. Fig. 11(b) is obtained from a cell with cemented grid and no prior heat treatment]. The observed current is lower and shows a highly inhomogeneous spatial distribution (probably caused by the spatial distribution of L_n). With increasing heat treatment the currents increase but only until they hit a plateau, presumably given by the high-field domain carrier density n_{II}. The plateaus widen and finally the entire cell shows the homogeneous current ceiling.

The best present estimate of the band model of CdS-Cu_2S solar cell is given in Fig. (11) (open-circuit conditions). In the Cu_2S the Fermi level is close to the top of the valence band with $p \simeq 5 \times 10^{19}$ cm^{-3}. The electron quasi-Fermi level is nearly 0.35 eV below the conduction band and drops very slightly (by 0.03 eV) towards the junction interface. (See Fig. 12.) The electron current flow is compensated by a hole flow (recombination current through the junction). At the outer surface probably a thin copper oxide layer with a larger band gap reduces surface recombination (a drift field of sufficient magnitude cannot be developed in the degenerate Cu_2S to achieve a significant reduction of surface recombination).

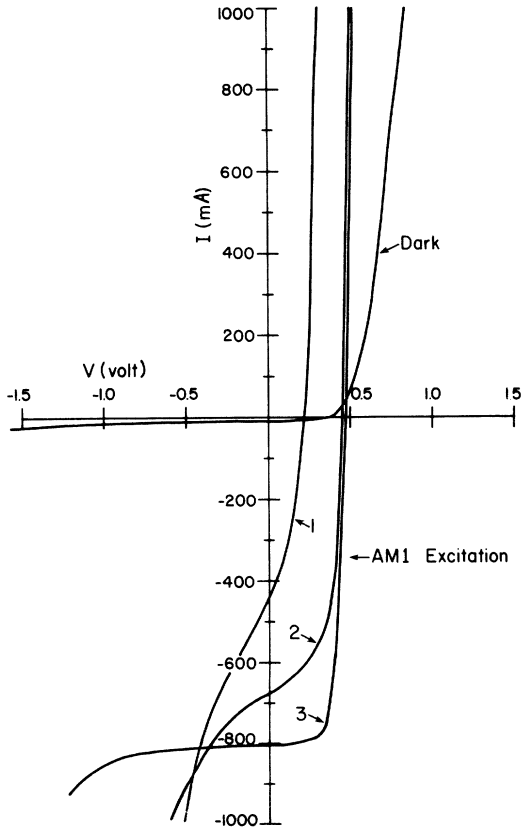

FIG. 10. Current-voltage characteristics (a) before and after successive heat treatments at 130 °C, 6 h (b) and (c) total of 12 h.

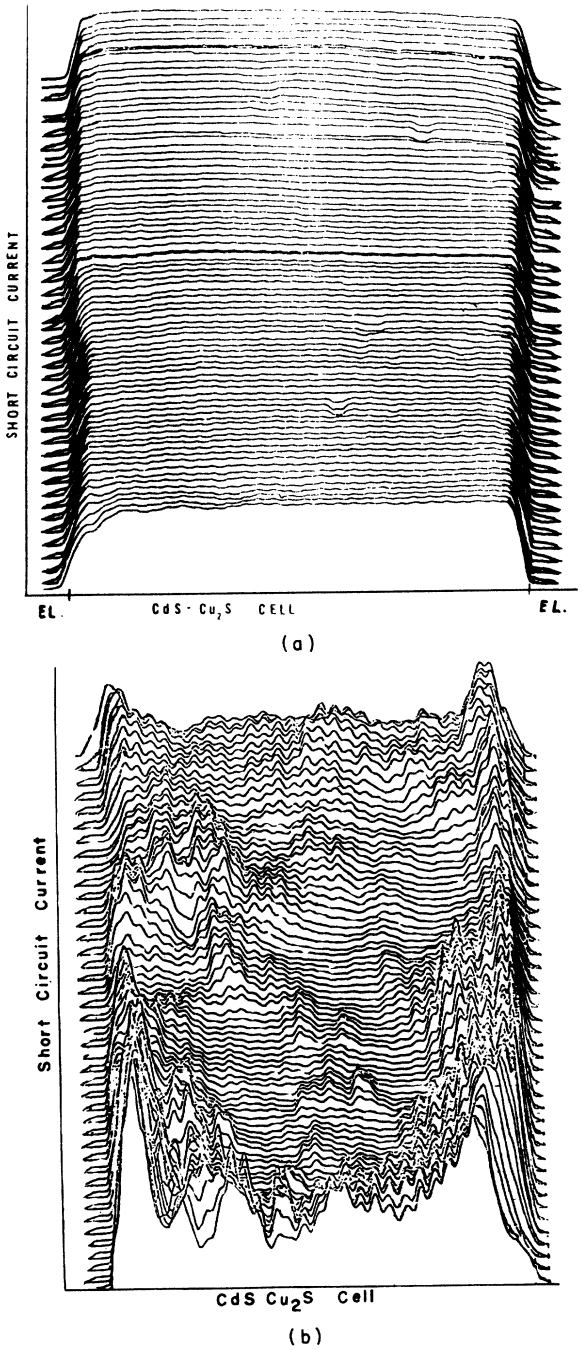

FIG. 11. Scanning light spot analysis of short-circuit current distribution (Ref. 24). (a) heat treated sample, (b) before heat treatment [0.2 times scale of (a)].

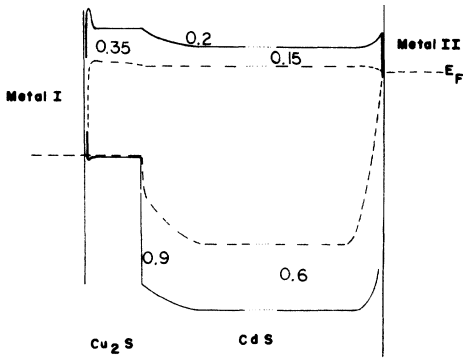

FIG. 12. Best present estimate of CdS-Cu_2S Band model. AM1 illumination, open-circuit condition.

The conduction bands of Cu_2S and CdS are joined without a potential jump. At the junction interface a negative space charge of almost 10^{12} cm^{-2} provides for the proper increase of field from the Cu_2S to the CdS from less than 10^{-2} V/cm to $\simeq 50$ kV/cm. The junction region in CdS has a width of approximately 0.3 μm (field dependent) and for open circuit conditions a diffusion potential of $\simeq 0.2$ V. The distance of the electron–quasi-Fermi level from the conduction band in the CdS bulk is $\simeq 0.15$ eV. The distance of the quasi-Fermi level for holes from the valence band is approximately 0.6 eV in the bulk and nearly 0.9 eV close to the junction interface [assuming continuity of j_p but no field quenching yet (open-circuit voltage case)]. The sloping of E_{F_n} to compensate for the hole current Eq. (23) is negligible (<1 meV).

The thermal activation energy for j_0, Eqs. (1) and (12) is in good agreement with $V_d + V_{oc} \simeq 0.85$ V. $j_{00} \simeq 10^4$ A/cm^2 is in order of magnitude in agreement with the experiment. However, the theoretical value for the open-circuit voltage as obtained from [see Eq. (12a)]

$$V_{oc} = E_g(Cu_2S) - \tilde{V}_d \tag{24}$$

is too large by about 0.3 V compared to the experimental values and assuming $E_{g1} = 1.2$ eV. One possibility for this discrepancy may be that the band gap for thermal excitation is smaller than the optical gap in Cu_2S (Franck-Condon shift). Another possibility is a band-gap reduction in Cu_2S because of high acceptor densities, or mechanical stress. More work needs to be done to clear up this discrepancy.

ACKNOWLEDGMENTS

Stimulating discussions with G. A. Dussel, H. C. Hadley, Jr., and J. Phillips are gratefully acknowledged. The permission to use the light scanner built by Dr. N. C. Wyeth is appreciated.

*Work supported in part by NSF Grant No. AER72-03478, formerly NSF/RANN/SE/GI-34872, and the ONR Grant No. N00014-71-C-0169.

[1]K. W. Böer, Proceedings of the 9th IEEE Photovoltaic Specialists Conference, Silver Springs, Maryland, May 2–4, 1972 (unpublished); K. W. Böer, Chem. Tech. 3, 394 (1973).

[2]Conference Proceedings, Summary, of International Workshop on CdS Solar Cells and Other Abrupt Heterojunctions, Newark, Delaware, April 30-May 2, 1975 report No. NSF/RANN-AER-75-15858 (unpublished).

[3]H. M. Windawi, Technical report No. NSF/RANN/AER-72-03478 A03/TR/75/1 and Proceedings of the Tenth IECEC Conference, Delaware, IEEE Cat. No. 75 CHO 983-7TAB, 1975 (unpublished).

[4]P. Brody, Proceedings of the International Workshop on CdS Solar Cells and Other Abrupt Heterojunctions, Newark, Delaware, April 30-May 2, 1975 report No. NSF/RANN-AER-75-15858 (unpublished).

[5]K. W. Böer, C. E. Birchenall, I. G. Greenfield, H. C. Hadley, Jr., T. L. Lu, L. Partain, J. E. Phillips, J. Schultz, and W. F. Tseng, Conference Record of the 10th IEEE Photovoltaic Specialists Conference, Palo Alto, Calif. November 13–15, 1973 (unpublished).

[6]L. R. Shiozawa *et al.*, Final Report, contract No. AF 33(615)-5224, June 1966-May 1969 (unpublished).

[7]T. S. teVelde and J. Dieleman, Philips Res. Rep. 28, 573 (1973).

[8]B. J. Moulder, Krist. Tech. 8, (7) 825 (1973).

[9]10% losses via reflection and 12% losses through the contact grid are assumed. g is assumed to be constant throughout the Cu_2S layer, its value is calculated from Ref. 10 with a weighted absorption coefficient average in the range $0.35 < \lambda < 1.05$ μm.

[10]H. Hadley, report No. NSF/RANN/SE/GI-34872/TR 74/3 (unpublished).

[11]Annual Report No. NSF/RANN/SE/GI-34872/PR/74/4 (unpublished).

[12]C. E. Birchenall and T. L. Lu, report No. NSF/RAN/SE/GI-34872 TR 73/7 (unpublished).

[13]G. A. Sullivan, Phys. Rev. 184, 796 (1969).

[14]K. W. Böer, Phys. Rev. 139, 1949 (1965).

[15]G. A. Dussel and K. W. Böer, Phys. Status Solidi 39, 375, 391 (1970).

[16]The CdS part of the cell may be regarded as the diode, connected to the Cu_2S part as the current generator, the connection of the two parts providing the proper boundary condition.

[17]K. W. Böer and P. L. Quinn, Phys. Status Solidi 17, 309 (1966).

[18]Curves 1 and 2 of Fig. 5 are also solutions of (14), however, since for curve 2 $j_n \simeq 0$ and for curve 1 $j_n < 0$ the logarithmic representation for the field of direction is not suitable.

[19]K. W. Böer and P. Voss, Phys. Rev. 171, 899 (1968).

[20]H. Hadley, P. Voss, and K. W. Böer, Phys. Status Solidi 11, K145 (1972).
[21]K. W. Böer and K. Bogus, Phys. Rev. 176, 899 (1968).
[22]K. W. Böer, G. Döhler, G. A. Dussel, and P. Voss, Phys. Rev. 169, 700 (1968).
[23]K. W. Böer and J. Phillips, Proceedings of the 9th IEEE Photovoltaic Specialist Conference, 1972 (unpublished).
[24]Method described by N. C. Wyeth in Ref. 2.